Nano Energy 100 (2022) 107500

Contents lists available at ScienceDirect

Nano Energy

journal homepage: www.elsevier.com/locate/nanoen

Untethered triboelectric patch for wearable smart sensing and energy harvesting

Dazhe Zhao [a], Kaijun Zhang [a], Yan Meng [c], Zhaoyang Li [a], Yucong Pi [a], Yujun Shi [a], Jiacheng You [a], Renkun Wang [a], Ziyi Dai [b], Bingpu Zhou [b], Junwen Zhong [a,*]

[a] Department of Electromechanical Engineering and Centre for Artificial Intelligence and Robotics, University of Macau, 999078, Macao Special Administrative Region of China

[b] Joint Key Laboratory of the Ministry of Education, Institute of Applied Physics and Materials Engineering, University of Macau, Avenida da Universidade, Taipa 999078, Macao Special Administrative Region of China

[c] Fujian Raynen Technology Co., Ltd., No. 89, Software Rd., Gulou District, Fuzhou, Fujian 350003, China

ARTICLE INFO

Keywords:
Wearable electronics
Triboelectric
Untethered
Self-powered sensor
Energy harvester

ABSTRACT

Wearable triboelectric devices have been widely used for sensing and energy harvesting applications, and further improving the compactness will enhance the convenience and comfortability. In this work, an easy-fabricated and compact untethered triboelectric patch is proposed with Polytetrafluoroethylene (PTFE) as triboelectric layer and human body as conductor. We find that the conductive characteristic of human body has negligible influence on the outputs, and the untethered triboelectric patch has good output ability and robustness. The proposed untethered triboelectric patches can work as sensor patches and energy harvester patches. Three typical applications are demonstrated, which are machine learning assisted objects distinguishing with accuracy up to 93.09–94.91 %, wireless communication for sending typical words to a cellphone, and human motions energy harvesting for directly powering electronics or charging an energy storage device.

1. Introduction

With the fast development of Internet of Things (IoT), wearable devices are drawing more and more attention in wide fields, such as healthy monitoring [1–5], epidemic protection [6,7], smart sensing [8–10], virtual reality (VR) and augmented reality (AR) [11–13], *etc*. As one of the important components of wearable devices, triboelectric nanogenerators (TENGs) first proposed in 2012 by Wang [14] show great superiority like battery-free, flexibility, low-cost, high-output, and easy-fabrication [15–17], which are competitive advantages for wearable devices. Therefore, TENGs are widely used in self-powered systems to overcome the limitations like limited lifetime, pollution problem, rigidity and bulkiness of traditional lithium-ion batteries [18]. In specific, TENGs are designed to extract electrical energy or signals from joint motions [19–21], eye blinks [22,23], even the heart pulses [24–26]. To obtain a higher output and more comfortable wearing experience, various structures are designed to provide a more convenient way for wearing or integrating on human body, such as patches that can well attach on human body [21,27], fiber structures with super flexibility and tiny weight [28,29], and textiles that are air-permeable and can be part of clothes [30,31], *etc*. However, most TENGs used in wearable devices need extra conductive wires attached on human body to connect with other electronic components, which will increase the redundancy of whole system and cause the inconvenience in working process. As is well known, human body is also a conductor [32,33]. For example, human body has been used as conductive media in harvesting electromagnetic or mechanical energy from ambient environment, which shows the possibility of transmitting electrical signal or power through human body to reduce the redundancy of the whole system [34–37]. An untethered TENG system using human body as conductor will be compact, miniaturized, and portable.

Herein, we propose an untethered triboelectric patch based on Polytetrafluoroethylene (PTFE) as triboelectric layer [29,38] and human body as conductor for connecting the external electronics. The untethered triboelectric patch can be easily integrated with human body for smart sensing and energy harvesting applications. Key advancements of this work include: **(i)** the untethered triboelectric patch is easy-fabricated and compact, and the conductive characteristic of human body has negligible influence on the outputs; **(ii)** the untethered triboelectric patch has good output stability, a device has output

* Corresponding author.
E-mail address: junwenzhong@um.edu.mo (J. Zhong).

https://doi.org/10.1016/j.nanoen.2022.107500
Received 27 April 2022; Received in revised form 29 May 2022; Accepted 10 June 2022
Available online 13 June 2022

variation of less than 5 % for continuous 18,000 rubbing cycles; **(iii)** together with machine learning method, objects distinguishing with the sensor patches attached on fingers is demonstrated, with accuracy of 93.09–94.91 % for distinguishing 11 objects when verified by multiple volunteers; **(iv)** wireless communication for transmitting typical words is realized by the sensor patches attached on fingers together with a miniaturized measuring circuit; **(v)** when attached on feet, the energy harvesting patches can harvest human motion energy for directly powering 16 LEDs or charging a capacitor to power a buzzer.

2. Results and discussion

2.1. Design strategy and working mechanism

The working mechanism of the untethered triboelectric patch is schematically shown in Fig. 1**a**. The patch is mainly composed of a PTFE electret layer integrated with a flexible substrate, and then it's attached to human skin. First, the PTFE layer is rubbed with external objects (normally a wood table) to generate negative electrostatic charges on the surface, profiting from the strong triboelectrification effect of PTFE. The electric charging process and the surface potential *versus* rubbing time curves are illustrated in Fig. S1. Rubbing time of 10 s with frequency of around 3–5 Hz is enough for fully charging the PTFE, with surface potential of ~ −1850 V. In fact, the untethered triboelectric patch is a single electrode mode triboelectric device with human body as a conductive path [39]. The outputs of the patch are also related to the properties of the testing objects, such as surface morphology, electrification, dielectricity, and conductivity, *etc*. Normally, the amplitude of the output currents is in micro-ampere level, which is not harmful or maybe helpful to human, such as accelerating wound healing [40,41]. The generated outputs can work as "signals" to make the patch as a sensor patch or as "electricity" to make the patch as an energy harvester patch (Fig. S2). In typical, applications of machine learning assisted object distinguishing (Fig. 1**b**), wireless communication (Fig. 1**c**), and human motion energy harvesting (Fig. 1**d**) are successfully demonstrated to prove the potential applications.

The resistance of human body mainly exists in human skin, and the skin resistance has a large range of variation. Compared with skin resistance, the bulk body resistance is much more stable and smaller, with a typical value of around 300–500 Ω [42]. From volunteer's test, we prove that the resistance between two hands of human body is less than 2 MΩ at normal situation, as shown in Fig. S3**.** This value is small enough that it cannot be considered as a dielectric layer. To prove this fact, a piece of CNTs/PDMS film with a value of about 2 MΩ mimicking human skin is placed on a copper electrode, then a square wave voltage with peak value of 100 V is applied on the electrode. Applied voltage and the surface potential of the CNTs/PDMS are monitored and shown in Fig. S4. Results prove that the surface potential of the CNTs/PDMS changes synchronously with the applied voltages and no opposite potential appears.

For the untethered triboelectric patch, one working cycle can be separated into a contact process and a separation process. Surface potential on skin and tissue fluctuates in these two processes due to electrostatic induction effect. During the contact process, surface potential on human body increases and becomes higher than the ground, and current will flow from human body to ground, as shown in Fig. 2**a**. During the separation process, surface potential on human body decreases and becomes lower than the ground, and current will flow from ground to human body, as shown in Fig. 2**b**. When the patch is attached on the index finger of right hand, surface potential of left hand during these two processes is shown in Fig. 2**c**. In this test, there is a loop between the patch and ground. The surface potential relative to the ground electrode of the electrometer is positive during the contact process and negative during the separation process. It should be noted that if we keep the contacting or pressing states, the surface potential of human body will finally decrease to zero because the surrounding environment is not absolutely insulated.

On the other hand, with a patch attached on the index finger of right hand, the positive probe of a current meter is linked to 3 positions of human body, which are left-hand palm (P4), neck (P3), and right-hand palm (P2), or directly linked to an Al electrode (P1) which is placed under PTFE layer to record the output characteristics, as indicated in Fig. 2**d**. The output characteristics of the 4 positions are very similar. The peak values of the outputs from 4 positions are close, and the output

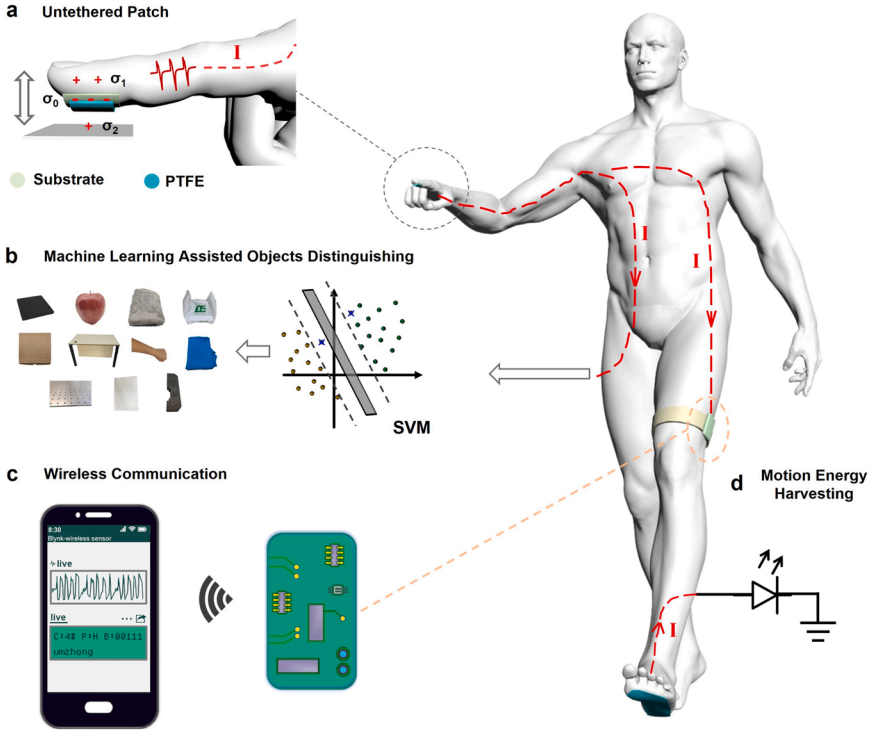

Fig. 1. Schematic diagram of the design strategy and typical applications of the untethered triboelectric patch. **(a)** Schematic diagram illustrating the basic working mechanism, signals or electricity from the patch are transmitted directly through human body to make the whole system without any conductive wire attached on human body. Typical applications for the untethered triboelectric patch in **(b)** machine learning assisted objects distinguishing, **(c)** wireless communication, and **(d)** motion energy harvesting. The algorithm used in machine learning is support vector machines (SVM).

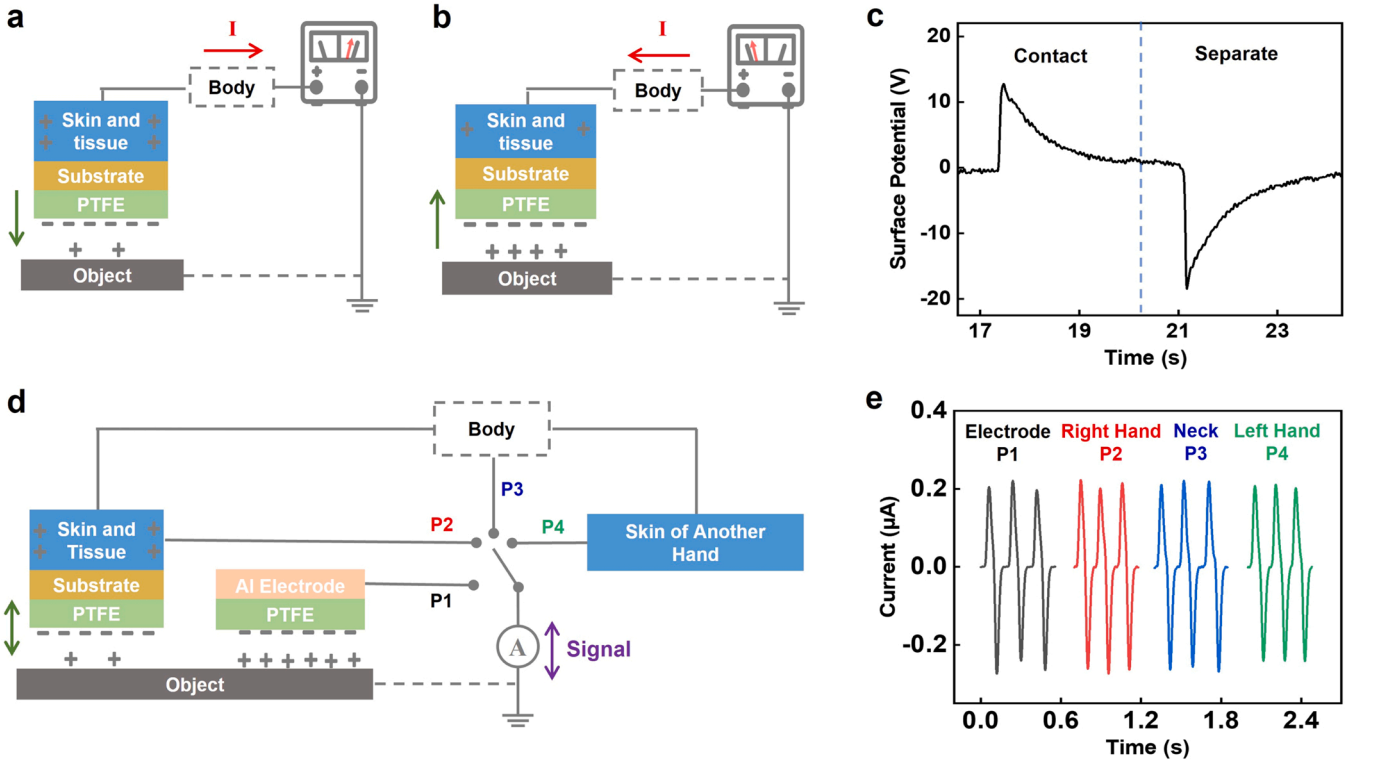

Fig. 2. Working mechanism of untethered triboelectric patch. Schematic diagram of **(a)** contact process and **(b)** separation process. (**c**) Surface potential of human body during the contact-separation process. The untethered triboelectric patch is attached to the right hand and the surface potential of left hand is measured. **(d)** Schematic diagram illustrating the output characteristics of 4 different positions. **(e)** Output characteristics for left-hand palm (P4), neck (P3), and right-hand palm (P2) and an Al electrode (P1) which is placed under PTFE layer, when a patch is attached on the index finger of right hand.

waves show a positive peak during the contact process and a negative peak during the separation process, as shown in Fig. 2**e**.

Above results prove that: (1) the electrical potential of the whole human body is the same and human body can be considered to be equipotential during the working process of our triboelectric patch; (2) human skin cannot be considered as a dielectric layer and has no effect on the electrostatic induction process; (3) conductive path of human body has negligible influence on the performances of the sensor patch. In fact, human body does have capacitance characteristic, with capacitance of 150–250 pF [36,43]. As shown in Fig. S5, human body is firstly off-connected to the current meter and the human body is charged by tapping the triboelectric patch, then the left hand touches with the positive probe of current meter for 3 times, and 3 low current peaks of ~ 0.1 μA are detected, proving that human body can store some charges. Actually, the conductivity of human body plays a key role in this work.

3. Output characterizations of the untethered sensor patch

The photo and cross-sectional Scanning Electron Microscope (SEM) image of an untethered triboelectric patch as a sensor patch are illustrated in Fig. 3**a**. A PTFE film with thickness of ~ 50 μm is integrated with a ~ 100 μm thick band-aid (as the flexible substrate) by the adhesion of a ~ 100 μm thick double-sided tape. The total thickness of the sensor patch is ~ 220 μm. The mechanical strength of the sensor patch is strong, which can withstand mechanical stress up to 8 MPa before broken (Fig. S6). Our patch can stand strain of 5.7 % when it starts to crack, and can stand strain of 260 % when it totally cracks. The effective size of the sensor patch is a key parameter determines the output performances. As shown in Fig. 3**b**, with wood table as a testing object, the output open-circuit voltage of the sensor patches increases with the effective size increasing, from ~ 19.24 V for 19 * 24 mm^2 to ~ 63.33 V for 95 * 24 mm^2. In this test, we increase the size of the sensor patches by attaching one or multiple devices with typical effective size of 19 * 24 mm^2 to human fingers and get the outputs by contacting and separating the sensor patch with a wood table by finger motions with frequency of around 3 Hz. If there are multiple triboelectric patches on the same human body, the human body is the same electrode for these devices. So, we cannot distinguish the signal from each device.

The electrostatic charges on the PTFE generated by the triboelectrification effect is also a key parameter determines the performances of sensor patch. The electrostatic charges can be characterized by measuring the surface potential [44]. After fully electric charged by rubbing with a wood table, the surface potential of PTFE layer of the sensor patch is as high as around −2000 V. However, discharging does occur in the following sensing process. As shown in Fig. 3**c**, when the sensor patch contacts with a testing object (like a wood table), the surface potential drops to −800 to −900 V and keeps stable in the following 10 min working time, as PTFE is a good electret material that can easily hold electrostatic charges [29]. Five charging and sensing cycles are repeated and the results are similar. Longer working time of 30 min also show the surface potential stability during the sensing process, as shown in Fig. S7. We also verify in Fig. 3**d** that the relative output intensity of a 19 * 24 mm^2 sensor patch keeps roughly stable during the testing time of 10 min, with average intensity variation less than 10 %. The output performances of each working minute are measured, and the input mechanical stimulations are from finger motions. Above results indicate that the output performances of the sensor patch can be recovered by repeated charging process and keep stable during normal working time with one charging process.

The influence of the human body resistance on outputs is investigated. The peak output current and voltage under loading resistance from 510 Ω to 400 MΩ of a 50 * 50 mm^2 sensor patch are shown in Fig. 3**e**. In this test, copper electrode with ignorable resistance is used and the loading resistance acts as the role of human body resistance, and regular pressing stimulation with frequency of 2 Hz and peak force of 1 N is applied to the sensor patch by a modal shaker (Fig. S8). When the

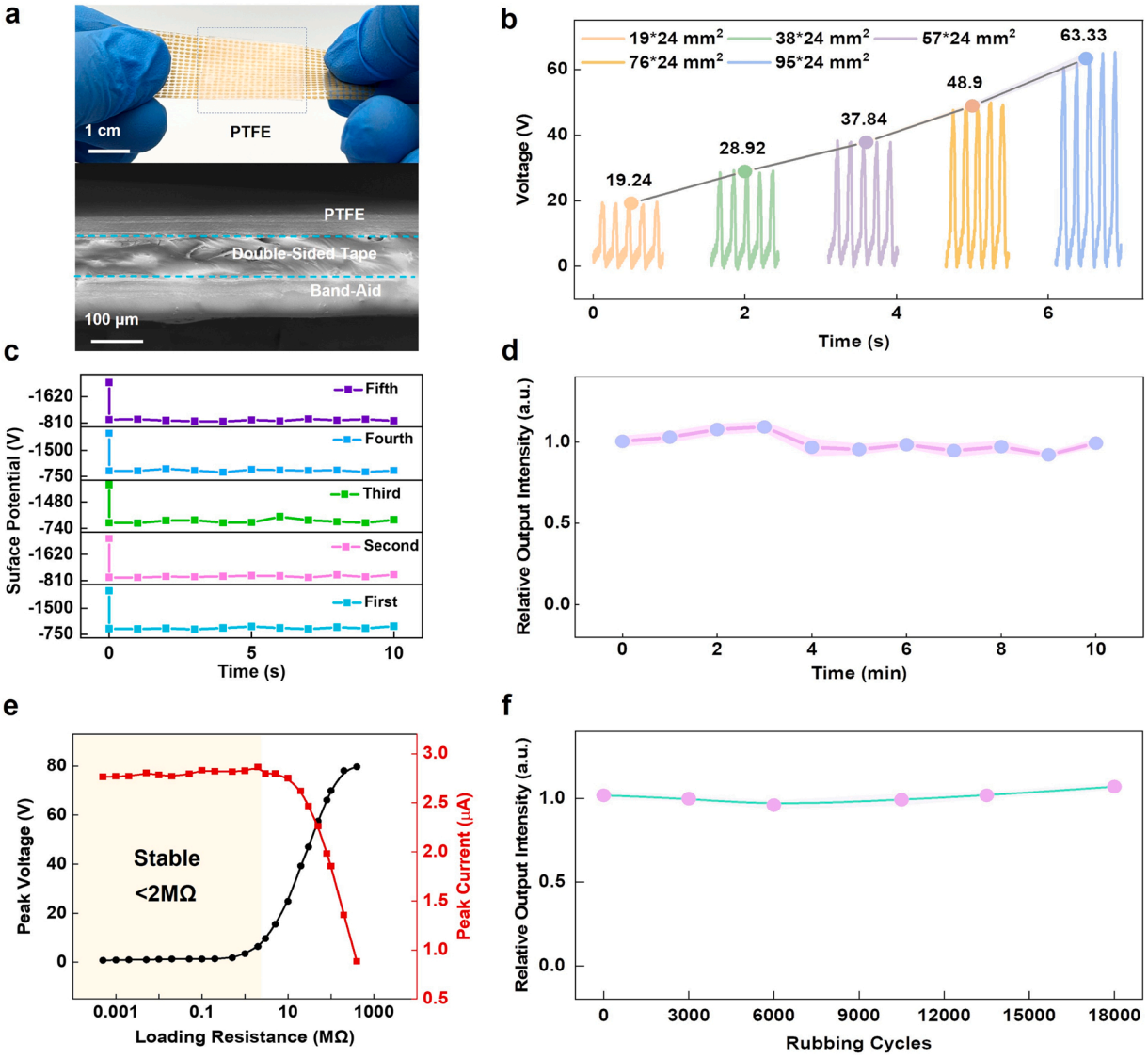

Fig. 3. Structure and outputs characterization of the untethered sensor patch. **(a)** Photo and cross-sectional SEM image illustrating the main components and structure of an untethered triboelectric patch as a sensor patch. **(b)** Output open-circuit voltage of sensor patches with various sizes, when testing with wood table. **(c)** Surface potential *versus* time curves of PTFE layer of the sensor patch during the sensing process, five charging and sensing cycles are repeated. **(d)** Relative output intensity of a sensor patch (19 * 24 mm^2) *versus* time curve after fully charged by rubbing with wood table, in which the sensor patch keeps working for 10 min **(e)** Peak output voltage and current of a sensor patch (50 * 50 mm^2) under various loading resistance, the sensor patch is stimulated by regular pressing stimulation with frequency of 2 Hz and peak force of 1 N. **(f)** Relative output intensity of a sensor patch (19 * 24 mm^2) after rubbing with wood table for various cycles, verifying the robustness under mechanical abrasion of the sensor patch.

loading resistance is less than 2 MΩ, the outputs have little variation, indicating that human body resistance with normal resistance less than 2 MΩ (Fig. S3) has negligible influence on the performances of the sensor patch. Meanwhile, the peak power output *versus* loading resistance curve is shown in Fig. S9. The peak value appears at ~50 MΩ, which also proves that the internal resistance of the sensor patch is very high (like other triboelectric devices [45]) and low loading resistance like human body resistance has slight influence of the outputs.

The robustness under mechanical abrasion of the sensor patch is studied by continuously rubbing a 19 * 24 mm^2 patch with a wood table up to 18,000 cycles, and the outputs are measured during the rubbing process, in which the input mechanical stimulations are also from finger motions. As shown in Fig. 3**f**, the relative output intensity keeps stable, with variation of average values less than 5 %. Above results prove that the sensor patch has strong abrasion resistance and long lifetime. Moreover, the outputs of the sensor patch under various relative humidity are illustrated in Fig. S10. The sensor patch still outputs peak open circuit voltage of ~ 8 V when the relative humidity is up to 90 %. It should be noted that the sensor patch is protected by the flexible substrate and will not directly contact with sweat to make it be in an extremely humid environment.

4. Machine learning assisted smart sensing application

One typical application of our untethered triboelectric patch is distinguishing various objects integrating with the machine learning algorithm, which is an efficient means for solving the classification problems. In specific, Support Vector Machine (SVM) is a commonly used machine learning approach for classifying or distinguishing the output signals of triboelectric sensors [46]. That's because SVM is more appropriate for dealing with the scenario with small amount of sample data with enough distinguishable features, when compared with other machine learning algorithms like convolutional neural network (CNN) [46,47]. As shown in Fig. 4**a**, a sensor patch is attached on an index

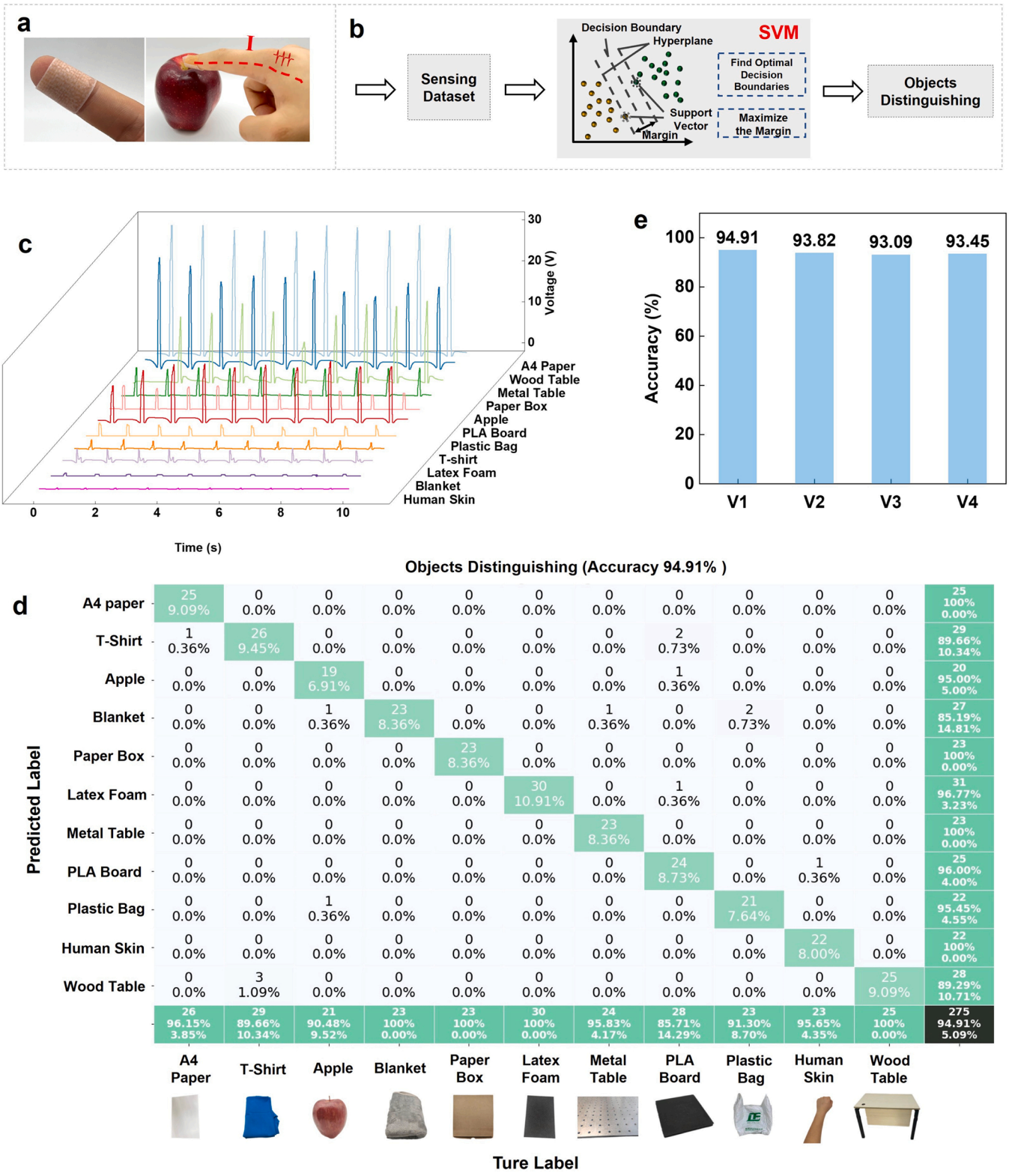

Fig. 4. Objects distinguishing based on the untethered sensor patch together with Support Vector Machine (SVM) algorithm. **(a)** Photo illustrating a sensor patch integrated with a finger and the objects distinguishing application. **(b)** Scheme illustrating the object distinguishing process based on SVM algorithm. **(c)** Outputs *versus* time curves for the sensor patch when sensing 11 objects, result of volunteer 1. **(d)** Confusion matrix of 11 objects distinguishing derived from SVM algorithm using the sensing dataset generated by the sensor patch, result of volunteer 1. **(e)** Distinguishing accuracy of 4 individual volunteers.

finger and then is used to touch testing objects like an apple. The response signals are transmitted through human body and then be recorded by the measuring system to form the sensing dataset which is applied for machine learning-assisted objects distinguishing. The basic principle of SVM is to find a decision boundary that can separate the data into classes, and the hyperplanes of these classes have maximum margin (Fig. 4**b**) [48].

In this test, we ask 4 volunteers to distinguish 11 objects. For

volunteer 1, the typical outputs of the sensor patch for testing 11 objects are illustrated in Fig. 4**c**. Only tens of cycles of outputs are collected for each object and the corresponding outputs have enough distinguishable features. One cycle of output is defined as a sample. The total 660 samples are randomly divided into training group (58.4 %) and testing group (41.6 %), and linear kernel is used in the training process, as shown in Fig. S11. The confusion map for distinguishing 11 objects is illustrated in Fig. 4**d**, showing a high accuracy up to 94.91 %. Moreover, as shown in Fig. 4**e**, the distinguishing accuracy for volunteers 2–4 are 93.82 %, 93.09 %, and 93.45 %, respectively, with corresponding outputs *versus* time curves and confusion matrix provided in Fig. S12. Such high distinguishing accuracy proves that our sensor patch can effectively distinguish various objects for individual users. The output characteristics for multiple users to sense the same testing objects are different, as the touching motions and the electrical response of different people may have big variation. In Fig. S13, we ask 5 volunteers to distinguish 4 testing objects of metal table, plastic bag, paper box, and wood table. When using the data of individual volunteer for machine learning, the average accuracy of the volunteers can reach up to 96.88 %. However, when mixing the data of multiple volunteers, the accuracy drops, 79.72 % for mixing 3 volunteers and 69.00 % for mixing 5 volunteers. These results indicate that the machine learning algorithm in this work is applicable for individual users. On the other hand, sensor patches are attached on two feet for distinguishing human motions, including "jump", "walk", and "run", with a high accuracy of 98.33 %, as shown in Fig. S14.

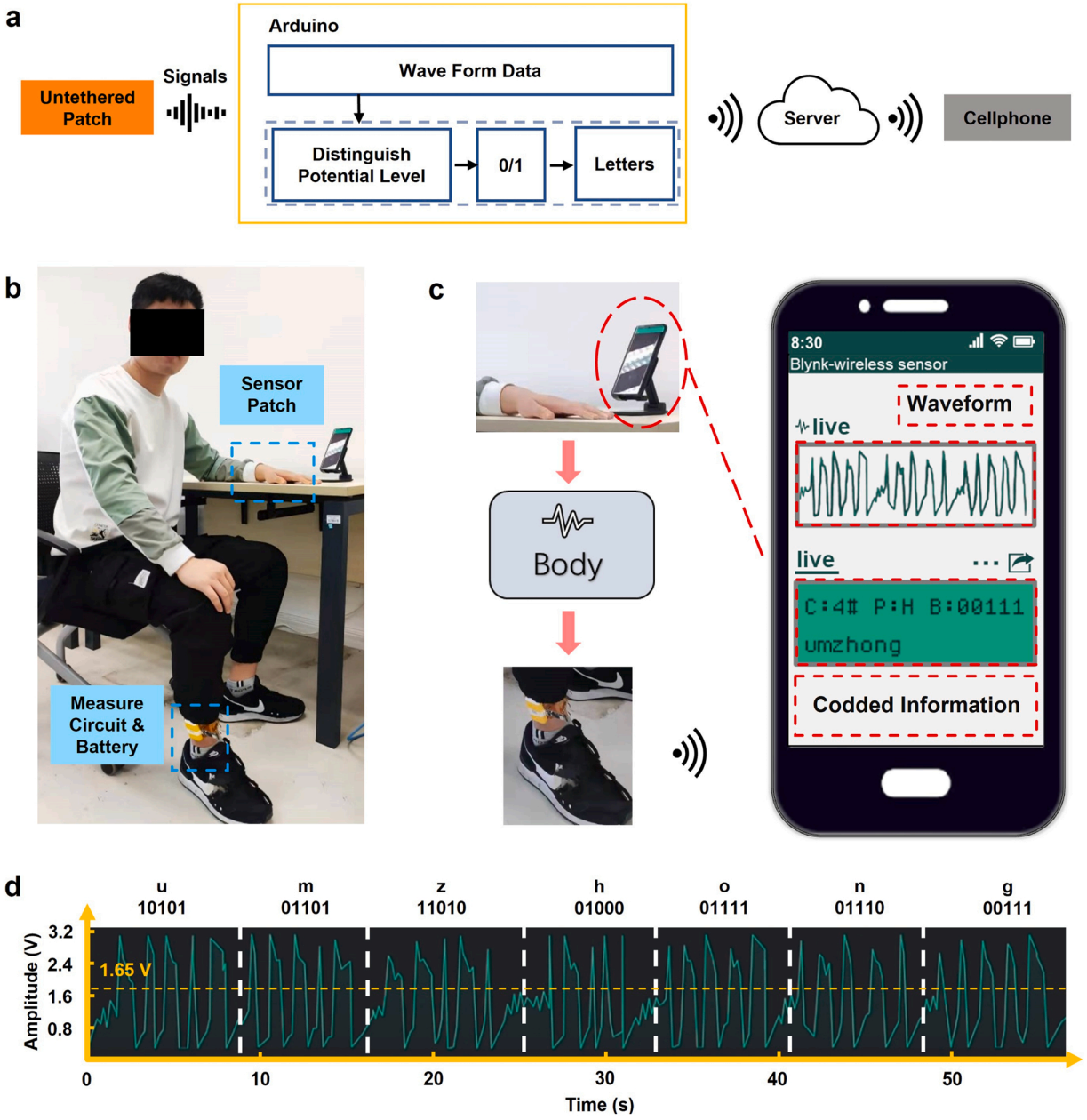

Fig. 5. Wireless communication system with the untethered sensor patch. **(a)** Block diagram of the wireless communication system, the codded information detected by the sensor patch is transmitted *via* human body to a measuring circuit powered by a battery, and then the codded information is wirelessly sent to and displayed on a cellphone *via* a server. **(b)** Photo illustrating the wireless communication system. **(c)** Transmitting process of the codded information and the main contents displayed on the cellphone. **(d)** Codded information of "umzhong" with the corresponding detected waveforms from the sensor patch and the codding rules for each letter.

5. Wireless communication application

Another typical application of our untethered triboelectric patch is the wireless communication together with a portable and battery-powered measuring circuit for data collection and a cellphone for displaying the sensing information. The components and working processes of the wireless communication system is illustrated in Fig. 5**a**. An Arduino board (Nano 33 IoT) as the measuring circuit is used for collecting and processing signals sensed by the patches, and then sending the sensing information to a cellphone *via* a cloud server. A specific wireless communication process is illustrated in Fig. 5**b** and Supporting Video 1, with detailed signal processing flowchart in Fig. S15. The signals are generated from the patches attached on the fingers and then transmitted to the readout circuit attached on the leg through conductive human body. After signal processing process in the Arduino, information coded by the regular fingers pressing motions are sent to the cellphone through Wi-Fi and both the live waveform and codded information are shown in the cellphone interface, as shown in Fig. 5**c**. In this wireless communication process, the output data points with a peak value larger than 1.65 V are defined as high potential level points. We directly set the number of high potential level points to define "0" or "1" states in the program of Arduino board. An output waveform with more than 7 high potential level points is defined as "1" state, while a waveform with less than 7 high level points is defined as "0" state. Generally, "1" or "0" state is determined by the peak width of an output waveform controlled by the holding time of a pressing motion. According to the codding rule in Supporting Table 1, all letters in alphabet can be codded with continues 5 states. For example, "10101″, "01101″, "11010″, "01000″, "01111″, "01110″, "00111″ are for "u", "m", "z", "h", "o", "n", "g", respectively, as shown in Fig. 5**d**.

Supplementary material related to this article can be found online at doi:10.1016/j.nanoen.2022.107500.

6. Energy harvesting application

The proposed untethered triboelectric patch also shows potential in harvesting energy from human motions and working as an energy harvester. As illustrated in Fig. 6**a**, with patches (80 *90 mm^2 for each foot) attached on two feet with black socks as the substrate, 16 LEDs can be directly powered by the collecting the energy generated by human motions. The energy harvester patches locate at the front and back parts of a foot to effectively contact with the ground (insert in Fig. 6**a**). With

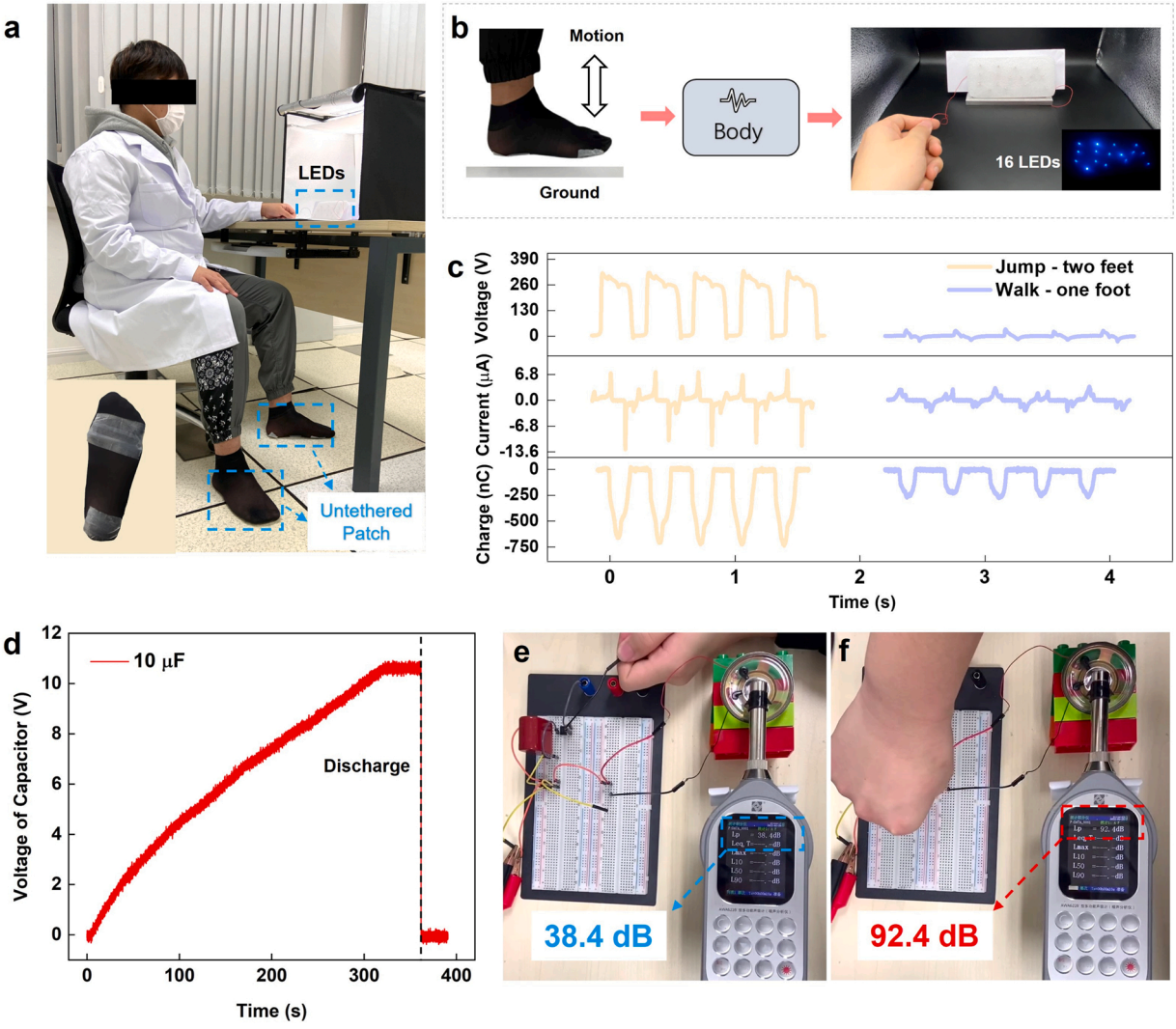

Fig. 6. Harvesting human motion energy with the untethered energy harvester patch. **(a)** Photo illustrating lighting up LEDs with untethered energy harvester patches integrated with two feet, insert shows the locations of the patches on the foot. **(b)** Electricity generation process and the 16 LEDs lighten by the electricity. **(c)** Output voltage, output current, and transferred charges generated by patches in jumping motions and walking motions. **(d)** Voltage *versus* time curves of a 10 μF capacitor when charged by walking motions and then discharged to power a buzzer. **(e)** Photo illustrating the charging process and background noise. **(f)** Photo illustrating the moment when the buzzer is powered and the maximum sound intensity generated by the buzzer.

the contact-separation motion between the patches and ground, electrical output is generated from the energy harvester patches and then transmitted through human body to the hand, finally illuminating a group of LEDs connected with the hand, as shown in Fig. 6**b** and Supporting Video 2. The output performances for typical jumping and walking motions are shown in Fig. 6**c**. For jumping motions, each electrical peak is from the patches on two feet and the frequency is around 3–4 Hz. For walking motion, each electrical peak is from the patches on one foot and the frequency is around 2–3 Hz. During jumping motion, the whole system is close to open-circuit condition. During walking motions, some part of skin of a foot will contact with the ground to form a loop as the black sock is porous and very thin. Thus, the whole system is not in an open-circuit condition, and there are positive and negative voltage peaks. The peak output voltage, peak output current, and transferred charges generated by the jumping motions are up to ~320 V, ~13 μA, and ~700 nC, respectively. The peak output voltage, peak output current, and transferred charges generated by the walking motions are much lower, which are ~30 V, ~3 μA, and ~250 nC, respectively.

Supplementary material related to this article can be found online at doi:10.1016/j.nanoen.2022.107500.

Using the energy harvesting patch, we can easily harvest human motion energy in our daily life, especially our energy harvesting patch is appropriate for indoor application. However, alternating current harvested in this way cannot be directly used to power electronics in most instances. Herein, a rectifier and a commercial capacitor (10 μF) are used to store energy generated by the untethered energy harvester patches, and then the accumulated energy can power a buzzer (Supporting Video 3). The charging and discharging curves are shown in Fig. 6**d** and equivalent circuit is illustrated in Fig. S16. In Fig. 6**d**, the 10 μF capacitor is charged by the walking motions with frequency of around 2–3 Hz, and the voltage across the capacitor is charged to ~10.6 V in ~310 s. Photos in Fig. 6**e** and Fig. 6**f** illustrate the charging and discharging processes for powering a buzzer. The background noise is around 40 dB, and the instantaneous maximum sound intensity increases to 92.4 dB when the buzzer is powered. These two demonstrations prove that our energy harvester patches can generate significant energy for directly powering electronics or charging energy storage devices.

Supplementary material related to this article can be found online at doi:10.1016/j.nanoen.2022.107500.

7. Conclusion

In summary, we have developed compact untethered patches based on the working mechanism of triboelectrification effect and electrostatic induction effect. The untethered triboelectric patches use PTFE as triboelectric layer and human body as conductor to improve the compactness and convenience of the whole system. We illustrate the working mechanism during the working process and find that the conductive characteristic of human body has negligible effect on the outputs. The untethered triboelectric patches have significant and stable output ability. As sensor patches or energy harvester patches, three typical applications are successfully demonstrated, which are machine learning assisted objects distinguishing, wireless communication, and human motion energy harvesting. Our work not only shows the potential applications of the untethered triboelectric patches, but also points out a strategy for obtaining more compact and integrated triboelectric wearable devices. For the demonstrations in this work, the triboelectric patches do not cover large area of skin, so it will not seriously affect the wearing comfort. It should be noted that better wearable experience will be achieved by using air-permeable and high-performance triboelectric layer in the future.

8. Experimental section

8.1. Fabrication of the untethered triboelectric patch

For the untethered triboelectric patch as a sensor, the flexible substrate is band-aid. The aseptic cotton layer is peeled off from a band-aid and then a PTEF film with thickness of 50 μm and size of 19 * 24 mm^2 is stuck to the surface of band-aid without aseptic cotton layer by double-sided tape. The fabricated patch can be attached on human skin by the adhesion part of the band-aid, making the PTFE layer contact with testing objects. For the untethered triboelectric patch as an energy harvester, the flexible substrate is black sock. A PTEF film with thickness of 50 μm and size of 80 * 90 mm^2 is stuck to the outer surface of a sock by double-sided tape.

8.2. Materials and devices characterization

The SEM image is probed by a high-resolution Field Emission Scanning Electron Microscope (Sigma FE-SEM, Zeiss Corporation, Germany). The surface potential of the samples is measured with an electrostatic voltmeter (Trek 347). The mechanical properties of the samples are tested by an electronic universal material testing machine (RGM-4005 T, Reger, China). The output current and voltage of the samples are measured by a Keithely 6514 electrometer and NI USB 6341 data acquisition system. The regular mechanical stimulation applied on the samples are provided by a Modal shaker (JZK-10, Sinocera Piezotronics, Inc. China) controlled by a YE1311 (Sinocera Piezotronics, China) sweep signal generator and a YE5872A (Sinocera Piezotronics, China) power amplifier. The study protocol is thoroughly reviewed and approved by the ethical committee of University of Macau (approval number BSERE21-APP022-FST). Informed signed consent for the volunteer tests is obtained from the volunteers prior to their participation in this study.

CRediT authorship contribution statement

Dazhe Zhao: Conceptualization, Methodology, Investigation, Writing – original draft. **Kaijun Zhang:** Conceptualization, Investigation. **Yan Meng:** Software; Investigation. **Zhaoyang Li:** Writing – original draft, Visualization. **Yucong Pi:** Investigation. **Yujun Shi:** Visualization. **Jiacheng You:** Investigation. **Renkun Wang:** Investigation. **Ziyi Dai:** Investigation; **Bingpu Zhou:** Writing – review & editing. **Junwen Zhong:** Methodology, Resources, Writing – original draft, Writing – review & editing, Funding acquisition.

Declaration of Competing Interest

The authors declare that they have no competing interests.

Acknowledgments

We acknowledge the funding support from the Science and Technology Development Fund, Macau SAR (FDCT) (File No. 0059/2021/AFJ, 0040/2021/A1), and Start Research Grant from University of Macau (SRG2021–00001-FST).

Appendix A. Supporting information

Supplementary data associated with this article can be found in the online version at doi:10.1016/j.nanoen.2022.107500.

References

[1] M. Zhu, Q. Shi, T. He, Z. Yi, Y. Ma, B. Yang, T. Chen, C. Lee, Self-powered and self-functional cotton sock using piezoelectric and triboelectric hybrid mechanism for healthcare and sports monitoring, ACS Nano 13 (2019) 1940–1952, https://doi.org/10.1021/acsnano.8b08329.

[2] E.O. Polat, G. Mercier, I. Nikitskiy, E. Puma, T. Galan, S. Gupta, M. Montagut, J. J. Piqueras, M. Bouwens, T. Durduran, G. Konstantatos, S. Goossens, F. Koppens, Flexible graphene photodetectors for wearable fitness monitoring, Sci. Adv. 5 (2019) eaaw7846, https://doi.org/10.1126/sciadv.aaw7846.

[3] S.M.A. Iqbal, I. Mahgoub, E. Du, M.A. Leavitt, W. Asghar, Advances in healthcare wearable devices, npj Flex. Electron 5 (2021) 9, https://doi.org/10.1038/s41528-021-00107-x.

[4] J. Zhong, Z. Li, M. Takakuwa, D. Inoue, D. Hashizume, Z. Jiang, Y. Shi, L. Ou, M.O. G. Nayeem, S. Umezu, K. Fukuda, T. Someya, Smart face mask based on an ultrathin pressure sensor for wireless monitoring of breath conditions, Adv. Mater. 34 (2022), 2107758, https://doi.org/10.1002/adma.202107758.

[5] G. Sinnapolu, S. Alawneh, Integrating wearables with cloud-based communication for health monitoring and emergency assistance, IEEE Internet Things J. 1–2 (2018) 40–54, https://doi.org/10.1016/j.iot.2018.08.004.

[6] H.C. Ates, A.K. Yetisen, F. Güder, C. Dincer, Wearable devices for the detection of COVID-19, Nat. Electron. 4 (2021) 13–14, https://doi.org/10.1038/s41928-020-00533-1.

[7] B. Ghatak, S. Banerjee, S.B. Ali, R. Bandyopadhyay, N. Das, D. Mandal, B. Tudu, Design of a self-powered triboelectric face mask, Nano Energy 79 (2021), 105387, https://doi.org/10.1016/j.nanoen.2020.105387.

[8] Q. Su, Q. Zou, Y. Li, Y. Chen, S.-Y. Teng, J.T. Kelleher, R. Nith, P. Cheng, N. Li, W. Liu, S. Dai, Y. Liu, A. Mazursky, J. Xu, L. Jin, P. Lopes, S. Wang, A stretchable and strain-unperturbed pressure sensor for motion interference–free tactile monitoring on skins, Sci. Adv. 7 (2021) eabi4563, https://doi.org/10.1126/sciadv.abi4563.

[9] S. Wang, Y. Fang, H. He, L. Zhang, C. Li, J. Ouyang, Wearable stretchable dry and self-adhesive strain sensors with conformal contact to skin for high-quality motion monitoring, Adv. Funct. Mater. 31 (2021), 2007495, https://doi.org/10.1002/adfm.202007495.

[10] H. Cheng-Yu, Z. Ahmed Abro, Z. Yi-Fan, R. Ahmed Lakho, An FBG-based smart wearable ring fabricated using FDM for monitoring body joint motion, J. Ind. Text. 50 (2021) 1660–1673, https://doi.org/10.1177/1528083719870204.

[11] E. Leroy, R. Hinchet, H. Shea, Multimode hydraulically amplified electrostatic actuators for wearable haptics, Adv. Mater. 32 (2020), 2002564, https://doi.org/10.1002/adma.202002564.

[12] J. Lee, H. Sul, W. Lee, K.R. Pyun, I. Ha, D. Kim, H. Park, H. Eom, Y. Yoon, J. Jung, D. Lee, S.H. Ko, Stretchable skin-like cooling/heating device for reconstruction of artificial thermal sensation in virtual reality, Adv. Funct. Mater. 30 (2020), 1909171, https://doi.org/10.1002/adfm.201909171.

[13] S. Mishra, Y.-S. Kim, J. Intarasirisawat, Y.-T. Kwon, Y. Lee, M. Mahmood, H.-R. Lim, R. Herbert, K.J. Yu, C.S. Ang, W.-H. Yeo, Soft, wireless periocular wearable electronics for real-time detection of eye vergence in a virtual reality toward mobile eye therapies, Sci. Adv. 6 (2020) eaay1729, https://doi.org/10.1126/sciadv.aay1729.

[14] F.-R. Fan, Z.-Q. Tian, Z. Lin Wang, Flexible triboelectric generator, Nano Energy 1 (2012) 328–334, https://doi.org/10.1016/j.nanoen.2012.01.004.

[15] Z.L. Wang, T. Jiang, L. Xu, Toward the blue energy dream by triboelectric nanogenerator networks, Nano Energy 39 (2017) 9–23, https://doi.org/10.1016/j.nanoen.2017.06.035.

[16] H. Wu, S. Wang, Z. Wang, Y. Zi, Achieving ultrahigh instantaneous power density of 10 MW/m2 by leveraging the opposite-charge-enhanced transistor-like triboelectric nanogenerator (OCT-TENG), Nat. Commun. 12 (2021) 5470, https://doi.org/10.1038/s41467-021-25753-7.

[17] Z. Zhang, J. Cai, High output triboelectric nanogenerator based on PTFE and cotton for energy harvester and human motion sensor, Curr. Appl. Phys. 22 (2021) 1–5, https://doi.org/10.1016/j.cap.2020.11.001.

[18] G. Khandelwal, N.P. Maria Joseph Raj, S.-J. Kim, Triboelectric nanogenerator for healthcare and biomedical applications, Nano Today 33 (2020), 100882, https://doi.org/10.1016/j.nantod.2020.100882.

[19] C. Pan, D. Liu, M.J. Ford, C. Majidi, Ultrastretchable, wearable triboelectric nanogenerator based on sedimented liquid metal elastomer composite, Adv. Mater. Technol. 5 (2020), 2000754, https://doi.org/10.1002/admt.202000754.

[20] Y. Yang, L. Chen, J. He, X. Hou, X. Qiao, J. Xiong, X. Chou, Flexible and extendable honeycomb-shaped triboelectric nanogenerator for effective human motion energy harvesting and biomechanical sensing, Adv. Mater. Technol. 7 (2022), 2100702, https://doi.org/10.1002/admt.202100702.

[21] P. Sun, N. Cai, X. Zhong, X. Zhao, L. Zhang, S. Jiang, Facile monitoring for human motion on fireground by using MiEs-TENG sensor, Nano Energy 89 (2021), 106492, https://doi.org/10.1016/j.nanoen.2021.106492.

[22] X. Pu, H. Guo, J. Chen, X. Wang, Y. Xi, C. Hu, Z.L. Wang, Eye motion triggered self-powered mechnosensational communication system using triboelectric nanogenerator, Sci. Adv. 3 (2017), e1700694, https://doi.org/10.1126/sciadv.1700694.

[23] D. Vera Anaya, T. He, C. Lee, M.R. Yuce, Self-powered eye motion sensor based on triboelectric interaction and near-field electrostatic induction for wearable assistive technologies, Nano Energy 72 (2020), 104675, https://doi.org/10.1016/j.nanoen.2020.104675.

[24] K. Meng, S. Zhao, Y. Zhou, Y. Wu, S. Zhang, Q. He, X. Wang, Z. Zhou, W. Fan, X. Tan, J. Yang, J. Chen, A wireless textile-based sensor system for self-powered personalized health care, Matter 2 (2020) 896–907, https://doi.org/10.1016/j.matt.2019.12.025.

[25] W. Fan, Q. He, K. Meng, X. Tan, Z. Zhou, G. Zhang, J. Yang, Z.L. Wang, Machine-knitted washable sensor array textile for precise epidermal physiological signal monitoring, Sci. Adv. 6 (2020) eaay2840, https://doi.org/10.1126/sciadv.aay2840.

[26] P. Bai, G. Zhu, Q. Jing, J. Yang, J. Chen, Y. Su, J. Ma, G. Zhang, Z.L. Wang, Membrane-based self-powered triboelectric sensors for pressure change detection and its uses in security surveillance and healthcare monitoring, Adv. Funct. Mater. 24 (2014) 5807–5813, https://doi.org/10.1002/adfm.201401267.

[27] S. Du, H. Suo, G. Xie, Q. Lyu, M. Mo, Z. Xie, N. Zhou, L. Zhang, J. Tao, J. Zhu, Self-powered and photothermal electronic skin patches for accelerating wound healing, Nano Energy 93 (2022), 106906, https://doi.org/10.1016/j.nanoen.2021.106906.

[28] L. Zhang, Q. Chen, X. Huang, X. Jia, B. Cheng, L. Wang, Y. Qin, Fiber-based electret nanogenerator with a semisupported structure for wearable electronics, ACS Appl. Mater. Interfaces 13 (2021) 46840–46847, https://doi.org/10.1021/acsami.1c16255.

[29] J. Zhong, Y. Zhang, Q. Zhong, Q. Hu, B. Hu, Z.L. Wang, J. Zhou, Fiber-based generator for wearable electronics and mobile medication, ACS Nano 8 (2014) 6273–6280, https://doi.org/10.1021/nn501732z.

[30] M. He, W. Du, Y. Feng, S. Li, W. Wang, X. Zhang, A. Yu, L. Wan, J. Zhai, Flexible and stretchable triboelectric nanogenerator fabric for biomechanical energy harvesting and self-powered dual-mode human motion monitoring, Nano Energy 86 (2021), 106058, https://doi.org/10.1016/j.nanoen.2021.106058.

[31] X. Tao, Y. Zhou, K. Qi, C. Guo, Y. Dai, J. He, Z. Dai, Wearable textile triboelectric generator based on nanofiber core-spun yarn coupled with electret effect, J. Colloid Interface Sci. 608 (2022) 2339–2346, https://doi.org/10.1016/j.jcis.2021.10.151.

[32] H.C. Burger, J.B. van MILAAN, Measurements of the specific resistance of the human body to direct current, Acta Med. Scand. 114 (1943) 584–607, https://doi.org/10.1111/j.0954-6820.1943.tb11253.x.

[33] S.B. Baumann, D.R. Wozny, S.K. Kelly, F.M. Meno, The electrical conductivity of human cerebrospinal fluid at body temperature, IEEE Trans. Biomed. Eng. 44 (1997) 220–223, https://doi.org/10.1109/10.554770.

[34] J. Li, Y. Dong, J.H. Park, J. Yoo, Body-coupled power transmission and energy harvesting, Nat. Electron. 4 (2021) 530–538, https://doi.org/10.1038/s41928-021-00592-y.

[35] R. Zhang, M. Hummelgård, J. Örtegren, M. Olsen, H. Andersson, Y. Yang, H. Zheng, H. Olin, The triboelectricity of the human body, Nano Energy 86 (2021), 106041, https://doi.org/10.1016/j.nanoen.2021.106041.

[36] R. Zhang, J. Örtegren, M. Hummelgård, M. Olsen, H. Andersson, H. Olin, Harvesting triboelectricity from the human body using non-electrode triboelectric nanogenerators, Nano Energy 45 (2018) 298–303, https://doi.org/10.1016/j.nanoen.2017.12.053.

[37] R. Zhang, M. Hummelgård, J. Örtegren, M. Olsen, H. Andersson, Y. Yang, H. Olin, Human body constituted triboelectric nanogenerators as energy harvesters, code transmitters, and motion sensors, ACS Appl. Energ. Mater. 1 (2018) 2955–2960, https://doi.org/10.1021/acsaem.8b00667.

[38] B. Wang, J. Zhong, Q. Zhong, N. Wu, X. Cheng, W. Li, K. Liu, L. Huang, B. Hu, J. Zhou, Sandwiched composite fluorocarbon film for flexible electret generator, Adv. Electron. Mater. 2 (2016), 1500408, https://doi.org/10.1002/aelm.201500408.

[39] Y. Yang, H. Zhang, J. Chen, Q. Jing, Y.S. Zhou, X. Wen, Z.L. Wang, Single-electrode-based sliding triboelectric nanogenerator for self-powered displacement vector sensor system, ACS Nano 7 (2013) 7342–7351, https://doi.org/10.1021/nn403021m.

[40] Y. Long, H. Wei, J. Li, G. Yao, B. Yu, D. Ni, A.L. Gibson, X. Lan, Y. Jiang, W. Cai, X. Wang, Effective wound healing enabled by discrete alternative electric fields from wearable nanogenerators, ACS Nano 12 (2018) 12533–12540, https://doi.org/10.1021/acsnano.8b07038.

[41] S.-H. Jeong, Y. Lee, M.-G. Lee, W.J. Song, J.-U. Park, J.-Y. Sun, Accelerated wound healing with an ionic patch assisted by a triboelectric nanogenerator, Nano Energy 79 (2021), 105463, https://doi.org/10.1016/j.nanoen.2020.105463.

[42] J. c Niple, J. p Daigle, L. e Zaffanella, T. Sullivan, R. Kavet, A portable meter for measuring low frequency currents in the human body, Bioelectromagnetics 25 (2004) 369–373, https://doi.org/10.1002/bem.20000.

[43] L. Yang, H. Liu, L. Xing, H. Ren, J. Zhang, Numerical calculations of human-body capacitance in mining tunnel environment, J. Phys. Conf. Ser. 418 (2013) 12002, https://doi.org/10.1088/1742-6596/418/1/012002.

[44] H. Li, Z. Guo, S. Kuang, H. Wang, Y. Wang, T. Wu, Z.L. Wang, G. Zhu, Nanocomposite electret with surface potential self-recovery from water dipping for environmentally stable energy harvesting, Nano Energy 64 (2019), 103913, https://doi.org/10.1016/j.nanoen.2019.103913.

[45] S. Niu, Z.L. Wang, Theoretical systems of triboelectric nanogenerators, Nano Energy 14 (2014) 161–192, https://doi.org/10.1016/j.nanoen.2014.11.034.

[46] M. Zhu, Z. Sun, Z. Zhang, Q. Shi, T. He, H. Liu, T. Chen, C. Lee, Haptic-feedback smart glove as a creative human-machine interface (HMI) for virtual/augmented reality applications, Sci. Adv. 6 (2020) eaaz8693, https://doi.org/10.1126/sciadv.aaz8693.

[47] T. Jin, Z. Sun, L. Li, Q. Zhang, M. Zhu, Z. Zhang, G. Yuan, T. Chen, Y. Tian, X. Hou, C. Lee, Triboelectric nanogenerator sensors for soft robotics aiming at digital twin applications, Nat. Commun. 11 (2020) 5381, https://doi.org/10.1038/s41467-020-19059-3.

[48] S. Kang, I. Kim, P.J. Vikesland, Discriminatory detection of ssDNA by surface-enhanced raman spectroscopy (SERS) and tree-based support vector machine (Tr-SVM), Anal. Chem. 93 (2021) 9319–9328, https://doi.org/10.1021/acs.analchem.0c04576.